Multiscaling analysis of the mean thermal energy balance equation in fully developed turbulent channel flow

Tie Wei*

Department of Mechanical Engineering, New Mexico Institute of Mining and Technology, Socorro, NM 87801, USA

(Received 9 April 2018; published 28 September 2018)

In this work we investigate properties of the mean thermal energy balance equation using a multiscaling analysis approach. The analysis of the mean thermal energy balance (MHB) equation and the mean momentum balance (MMB) equation are presented side by side to better demonstrate the similarities and differences between the two. The main findings of this work include, first, the multiscaling for the MHB equation are similar to those for the MMB equation in the outer layer, mesolayer, and log layer. Péclet number $\mathrm{Pe}_\tau = \mathrm{PrRe}_\tau$ in the MHB equation is the counterpart of Re_τ in the MMB equation. Here $\mathrm{Pr} \equiv \nu/\alpha$ denotes the Prandtl number of the fluid, which is the ratio between the kinematic viscosity ν and the molecular thermal diffusivity α. $\mathrm{Re}_\tau = \delta u_\tau/\nu$ is the Reynolds number of the flow defined with the channel half-height δ and the friction velocity u_τ. In the outer layer, mesolayer, and log layer, the shapes of the mean temperature and the mean velocity are very similar, and the shapes of the wall-normal turbulent transport of heat and momentum are also similar. Second, the molecular thermal diffusion sublayer is strongly influenced by the Prandtl number. At low Prandtl number ($\mathrm{Pr} < 1$), the thickness of the molecular thermal diffusion sublayer is $y_{l_t} = O(\frac{1}{\mathrm{Pr}^{1/2}}\frac{\nu}{u_\tau})$ or $y^+_{l_t} = O(\frac{1}{\mathrm{Pr}^{1/2}})$, a proper scaling for the wall-normal distance is $\mathrm{Pr}^{1/2}y^+$ where $y^+ = y/(\nu/u_\tau)$ is the inner-scaled wall-normal distance, and a relevant Péclet number is $\mathrm{Pr}^{1/2}\mathrm{Re}_\tau$. At very low Prandtl number ($\mathrm{Pr} \ll 1$), the molecular thermal diffusion sublayer becomes much thicker than the viscous sublayer (molecular momentum diffusion sublayer). At large Prandtl number ($\mathrm{Pr} > 1$), the thickness of the molecular thermal diffusion sublayer is $y^+_{l_t} = O(\frac{1}{\mathrm{Pr}^{1/3}})$, a proper scaling for the wall-normal distance is $\mathrm{Pr}^{1/3}y^+$, and a relevant Péclet number is $\mathrm{Pr}^{1/3}\mathrm{Re}_\tau$. At very high Prandtl number ($\mathrm{Pr} \gg 1$), the molecular thermal diffusion sublayer becomes much thinner than the viscous sublayer. Third, to be consistent with the scaled MHB equation, the "log law" for the mean temperature is presented using an inner-scaled wall-normal distance $y/(\alpha/u_\tau) = \mathrm{Pr}y^+$. The main effect of the Prandtl number is the shifting of the additive constant in the log law, due to the thickness of the molecular thermal diffusion sublayer and buffer layer. Fourth and finally, Zagarola-Smits-style scaling is applied to the mean velocity and the mean temperature deficit in the outer layer. An interpretation of the Zagarola-Smits-style scaling is provided. At sufficiently high Reynolds number and Péclet number, the Zagarola-Smits-style scaling is shown to be equivalent to the traditional scaling.

DOI: 10.1103/PhysRevFluids.3.094608

I. INTRODUCTION

Heat transfer in fluid flowing through parallel channels is one of the canonical flows most widely studied in physical laboratories and numerical simulations. The flow is driven by an imposed pressure gradient, and the heat transfer is maintained by a temperature difference between the

*tie.wei@nmt.edu

 ©2018 American Physical Society

channel walls and the fluid. Two common thermal boundary conditions used in physical experiments or numerical simulations are constant wall temperature or constant wall heat flux. Despite its simple geometry and numerous experimental, analytical, and numerical studies, however, our understanding of heat transfer in turbulent channel flow is still incomplete.

Over the past 20 years, numerical simulation, especially direct numerical simulation (DNS), has become an invaluable tool in investigating the fundamental nature of turbulent heat transfer [1–13]. Quantities that are difficult or impossible to measure in physical laboratories can be easily computed in numerical simulations. However, DNS has been limited by computing power to a moderate Reynolds number range between $\mathrm{Re}_\tau = 150$ [5] and $\mathrm{Re}_\tau = 4000$ [13], and a moderate Prandtl number range between $\mathrm{Pr} = 0.025$ and $\mathrm{Pr} = 10$ [6]. Despite the limited Reynolds number and Prandtl number range, DNS data have been essential in shedding light on the underlying physics in heat transfer in turbulent wall-bounded flows, and the data are also critical in assessing multiscaling analyses of turbulent heat transfer.

Using a scaling patch analysis approach [14,15], an alternative framework for describing the structure of turbulent wall-bounded flow and turbulent heat transfer has been developed [16,17]. Traditionally, turbulent wall-bounded flows are divided into four layers: a viscous sublayer, a buffer layer, a log layer, and an outer layer [18–20]. Based on the ratio between the turbulence term and the viscous term in the mean momentum equation and mean energy equation, the scaling patch analysis also divides the turbulent wall-bounded flows into four layers: a viscous sublayer, a mean momentum or heat balance layer, a mesolayer, and an outer layer [16,17]. The scaling patch analysis of the mean thermal energy balance equation has been further developed in Refs. [21–23].

Scaling of the mean temperature in convective turbulent boundary layers has been investigated by Wang *et al.* [24] using a variant of the similarity theory by George and Castillo [25]. Seena and Afzal investigated the mean momentum and thermal balance in fully developed turbulent channel flow using matched asymptotic expansions [26]. Their analysis also reveals the existence of an intermediate layer with its own characteristic scaling, between the traditional inner and outer layers. Using a function of a series of logarithmic functions in the mesolayer, Seena and Afzal presented closure models of Reynolds shear stress and Reynolds heat flux [27].

The goal of this paper is to gain insight into properties of heat transfer in turbulent wall-bounded flows by identifying proper scaling for the mean thermal energy equation, in particular to elucidate the role of Prandtl number and Reynolds number on the multiscaling of different layers. Another goal of this work is to minimize the number of scaled variables and simplify notation in studying the mean thermal energy equation.

The rest of the paper is organized as follows. In Sec. II the instantaneous and mean equations for the thermal energy and momentum, as well as the boundary conditions, are presented. To better match the boundary conditions, a transformed temperature is introduced. In Sec. III a multiscaling analysis of the mean thermal energy equation is presented for the outer layer, log layer, molecular diffusion sublayer, and mesolayer. We start with the outer layer to establish a proper scaling for the wall-normal turbulent transport of heat. Section IV gives the summary and conclusions.

II. GOVERNING EQUATIONS

To better demonstrate the analogy between the thermal energy equation and the momentum equation, we will present the two equations side by side. In each case, the left side is related to the momentum equation and will be referred to as Eq. (a), and the right side is related to the thermal energy equation and will be referred to as Eq. (b).

The instantaneous streamwise momentum equation and the instantaneous thermal energy equation for incompressible flow read [19,20]

$$\frac{\partial \widetilde{u}_i}{\partial t} + \widetilde{u}_j \frac{\partial \widetilde{u}_i}{\partial x_j} = -\frac{1}{\rho}\frac{\partial \widetilde{p}}{\partial x_i} + \nu \frac{\partial^2 \widetilde{u}_i}{\partial x_j^2}; \quad \frac{\partial \widetilde{T}}{\partial t} + \widetilde{u}_j \frac{\partial \widetilde{T}}{\partial x_j} = \alpha \frac{\partial^2 \widetilde{T}}{\partial x_j^2}. \tag{1}$$

In this work we follow notation of Tennekes and Lumley for decomposing the instantaneous quantities [19]. The tilde denotes instantaneous quantity, upper case letter denotes its mean, and lower case denotes its fluctuation. For example, in $\widetilde{u}_i = U_i + u_i$, $\widetilde{u}_i$ is the instantaneous velocity component in the i direction, U_i is its mean, and u_i is its fluctuation. Similarly, in $\widetilde{T} = T + t$, $\widetilde{T}$ is the instantaneous temperature, T is the mean temperature, and t is the fluctuation temperature. In Eq. (1) t denotes time, and ρ is the fluid density.

In this work, we focus on the fully developed turbulent channel flow with constant wall heat flux, $q_w = \text{const}$. By "fully developed," we mean both hydrodynamically and thermally fully developed. In fully developed turbulent channel heat transfer with constant wall heat flux, the mean temperature, the wall temperature, and the mixed mean temperature all increase linearly in the x direction. The mean pressure gradient and the mean temperature gradient in the x direction can be found as [28,29]

$$-\frac{1}{\rho}\frac{\partial P}{\partial x} = \frac{u_\tau^2}{\delta}; \quad \frac{\partial T}{\partial x} = \frac{dT_w}{dx} = \frac{dT_m}{dx} = \frac{u_\tau}{U_b}\frac{\theta_\tau}{\delta}, \tag{2}$$

where u_τ is defined by the wall shear stress τ_w as $u_\tau = \sqrt{\tau_w/\rho}$ and is commonly called friction velocity. θ_τ is defined by the wall heat flux as $\theta_\tau = q_w/(\rho C_p u_\tau)$ where C_p is the heat capacity of the fluid. θ_τ was first introduced by Squire, who called it friction temperature [30]. T_w is the wall temperature. $U_b = (\int_0^\delta U dy)/\delta$ is the bulk mean velocity, and $T_m = (\int_0^\delta UT dy)/(\int_0^\delta U dy)$ is the mixed mean temperature.

For fully developed turbulent channel flows, the mean momentum balance (MMB) equation and the mean thermal energy equation can be expressed as

$$0 = \frac{u_\tau^2}{\delta} + \nu\frac{\partial^2 U}{\partial y^2} + \frac{\partial(-\langle vu\rangle)}{\partial y}; \quad 0 = -U\frac{\partial T}{\partial x} + \alpha\frac{\partial^2 T}{\partial y^2} + \frac{\partial(-\langle vt\rangle)}{\partial y}, \tag{3}$$

where $-\langle vu\rangle$ denotes wall-normal turbulent transport of streamwise momentum, and $-\langle vt\rangle$ denotes wall-normal turbulent transport of heat. Angle brackets denote averaging. For brevity, we will call the mean thermal energy balance equation or the mean heat balance equation the MHB equation in the following.

The boundary conditions corresponding to Eq. (3) at $y = 0$ (channel wall) and $y = \delta$ (channel centerline), respectively, are

$$y = 0: \quad U = 0, \ \nu\frac{\partial U}{\partial y} = u_\tau^2, \ -\langle vu\rangle = 0; \quad T = T_w, \ -\alpha\frac{\partial T}{\partial y} = u_\tau\theta_\tau, \ -\langle vt\rangle = 0, \tag{4}$$

$$y = \delta: \quad U = U_c, \ \nu\frac{\partial U}{\partial y} = 0, \ -\langle vu\rangle = 0; \quad T = T_c, \ -\alpha\frac{\partial T}{\partial y} = 0, \quad -\langle vt\rangle = 0. \tag{5}$$

U_c and T_c are the mean velocity and the mean temperature at the channel centerline, respectively.

Boundary conditions at the channel centerline ($y = \delta$) in Eq. (5) show close analogies between the MHB equation and the MMB equation. However, the boundary conditions at the channel wall ($y = 0$) in Eq. (4) show differences between the MHB equation and the MMB equation. Specifically, the no-slip boundary condition for the velocity results in $U|_{y=0} = 0$, and the no-slip boundary condition for the temperature results in $T|_{y=0} = T_w$.

In many numerical simulations and experimental studies of channel heat transfer, heat transfer is established by adding heat through hotter channel walls, as sketched in Fig. 1. Hence fluid has the highest temperature at the wall and lower temperature at the channel centerline. To formally match the wall boundary conditions in Eq. (4), a transformed temperature is introduced as

$$\widetilde{\theta} = T_w - \widetilde{T}. \tag{6}$$

The mean temperature, its derivative, the fluctuation temperature, and the wall-normal turbulent transport of heat using the original temperature and the transformed temperature are related to each

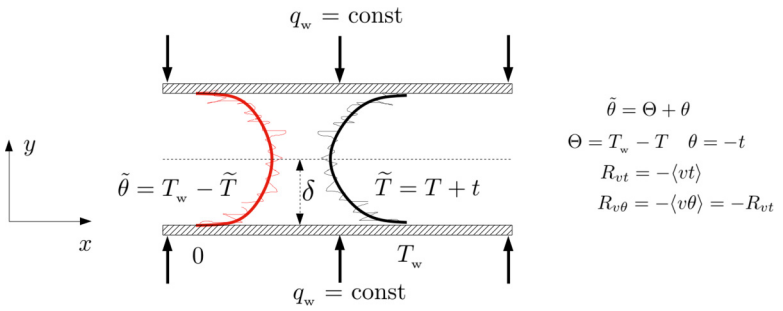

FIG. 1. Sketch of a parallel channel flow heated with constant flux. $\widetilde{T}$ is the instantaneous temperature; $\widetilde{\theta}$ is the transformed temperature.

other, respectively, as

$$\Theta = T_w - T; \quad \frac{\partial T}{\partial y} = -\frac{\partial \Theta}{\partial y}; \quad \theta = -t; \quad -\langle vt \rangle = \langle v\theta \rangle. \tag{7}$$

Note that the transformed mean temperature Θ varies only in the wall-normal y direction, not in the x direction, much like U. Using the transformed temperature, the MHB equation becomes

$$0 = -\frac{u_\tau \theta_\tau}{\delta U_b} U - \alpha \frac{\partial^2 \Theta}{\partial y^2} + \frac{\partial(\langle v\theta \rangle)}{\partial y}. \tag{8}$$

For brevity, we denote the wall-normal turbulent transport of streamwise momentum as $R_{vu} = -\langle vu \rangle$, and the wall-normal turbulent transport of heat as $R_{v\theta} = -\langle v\theta \rangle$. The MMB equation and the MHB equation using the transformed temperature can then be written as

$$0 = \frac{u_\tau^2}{\delta} + \nu \frac{\partial^2 U}{\partial y^2} + \frac{\partial R_{vu}}{\partial y}; \quad 0 = \frac{u_\tau \theta_\tau}{\delta} \frac{U}{U_b} + \alpha \frac{\partial^2 \Theta}{\partial y^2} + \frac{\partial R_{v\theta}}{\partial y}, \tag{9}$$

and the corresponding boundary conditions are

$$y = 0: \quad U = 0, \quad \nu \frac{\partial U}{\partial y} = u_\tau^2, \; R_{vu} = 0; \quad \Theta = 0, \quad \alpha \frac{\partial \Theta}{\partial y} = u_\tau \theta_\tau, \; R_{v\theta} = 0, \tag{10}$$

$$y = \delta: \quad U = U_c, \; \nu \frac{\partial U}{\partial y} = 0, \quad R_{vu} = 0; \quad \Theta = \Theta_c, \; \alpha \frac{\partial \Theta}{\partial y} = 0, \quad R_{v\theta} = 0. \tag{11}$$

Equations (10) and (11) clearly show analogies in boundary conditions between the MHB equation and the MMB equation.

Equations (9a) and (9b) show that the balance of the MMB equation and the MHB equation are both established by three terms: a driving or source term, a molecular diffusion term, and a turbulence term. In the MMB equation (9a), the driving "force" is the first term, which is the imposed pressure gradient. The second term comes from the molecular diffusion and is negative across the whole channel. In other words, the molecular diffusion term is always a "sink" term. The last term is the gradient of wall-normal turbulent transport of momentum, and this term changes sign at the R_{vu} peak location y_{mm}. Between the channel wall and y_{mm}, this turbulence term is positive and serves as a "source" term. Between y_{mm} and the channel centerline, this turbulence term becomes negative and acts as a "sink" term.

Similarly, the first term in the MHB Eq. (9b), originating from the mean advection, is positive across the whole channel and serves as a driving or source term. The second term is the molecular diffusion term and is negative throughout the channel, acting as a "sink" term. The third term is the turbulence term and changes sign at the $R_{v\theta}$ peak location y_{mt}. Between the channel wall and

y_{mt}, this turbulence term is positive and serves as a "source" term. Between y_{mt} and the channel centerline, this turbulence term becomes negative and acts as a "sink" term.

In the next section, we will perform multiscaling analysis of the MHB Eq. (9b). We will also present the corresponding multiscaling of the MMB equation, because it is more familiar, and offers interesting comparison with the MHB equation.

III. MULTISCALING ANALYSIS

It is known that the characteristic length scale, velocity scale, and temperature scale vary in different layer of a turbulent channel flow [18]. To determine a proper scaling for different layer of turbulent channel flow, therefore, it is crucial to identify proper scales for the wall-normal distance, the mean velocity and temperature, and the turbulent terms.

In the following we present multiscaling analysis for the outer layer, log layer, molecular diffusion sublayer, and mesolayer. For each layer, proper length scale, velocity scale, and temperature scale are identified, and the role of Prandtl number and Péclet number are determined.

A. Scaling in the outer layer

In the outer layer of turbulent channel flows, a proper and natural length scale is the channel half-height $l_o = \delta$. Normalized by l_o, the outer-scaled wall-normal distance is denoted as

$$\eta = \frac{y}{l_o} = \frac{y}{\delta}. \tag{12}$$

Traditionally, the mean streamwise velocity U and the wall-normal turbulent transport of streamwise momentum R_{vu} are normalized by the friction velocity u_τ. Similarly, the traditional scaling of the mean temperature Θ and the wall-normal turbulent transport of heat $R_{v\theta}$ also employs the friction temperature and velocity as

$$U^+ = \frac{U}{u_\tau}, \quad R^+_{vu} = \frac{R_{vu}}{u^2_\tau}; \quad \Theta^+ = \frac{\Theta}{\theta_\tau}, \quad R^+_{v\theta} = \frac{R_{v\theta}}{u_\tau \theta_\tau}. \tag{13}$$

Using the scaling in Eqs. (12) and (13), the outer-scaled MMB equation and MHB equation for the outer layer of the turbulent channel can be written as

$$0 = 1 + \frac{1}{\mathrm{Re}_\tau}\frac{\partial^2 U^+}{\partial \eta^2} + \frac{\partial R^+_{vu}}{\partial \eta}; \quad 0 = \frac{U^+}{U^+_b} + \frac{1}{\mathrm{Pe}_\tau}\frac{\partial^2 \Theta^+}{\partial \eta^2} + \frac{\partial R^+_{v\theta}}{\partial \eta}, \tag{14}$$

where $\mathrm{Pe}_\tau = \mathrm{Re}_\tau \mathrm{Pr}$ is the Péclet number defined with friction velocity.

1. Outer scaling of R_{vu} and $R_{v\theta}$

To check the validity of the outer-scaled Eq. (14), we first present the outer-scaled profiles of R_{vu} and $R_{v\theta}$ in Fig. 2. Profiles of R^+_{vu} from different Reynolds numbers collapse well in the channel outer region $\eta \gtrsim 0.2$, as shown in Fig. 2(a). As Reynolds number increases, the R_{vu} peak location moves monotonically toward smaller η, and the peak value of R^+_{vu} monotonically increases towards a value of 1. The case at $\mathrm{Re}_\tau = 180$, not surprisingly, shows low Reynolds number effect.

In comparison, Fig. 2(b) displays a more complicated variation of $R_{v\theta}$. This is not surprising, because $R_{v\theta}$ is affected by two parameters: the Prandtl number of the fluid and the Reynolds number of the flow. As shown in Eqs. (14a) and 14(b), Pe_τ in the MHB equation is the counterpart of Re_τ in the MMB equation. Indeed, Fig. 2(b) shows that the peak $R_{v\theta}$ location also moves to smaller η with increasing Pe_τ, and the peak value of $R^+_{v\theta}$ approaches 1 as Pe_τ increases. The scaling for the $R_{v\theta}$ peak location and peak value will be discussed below in the subsection on the mesolayer.

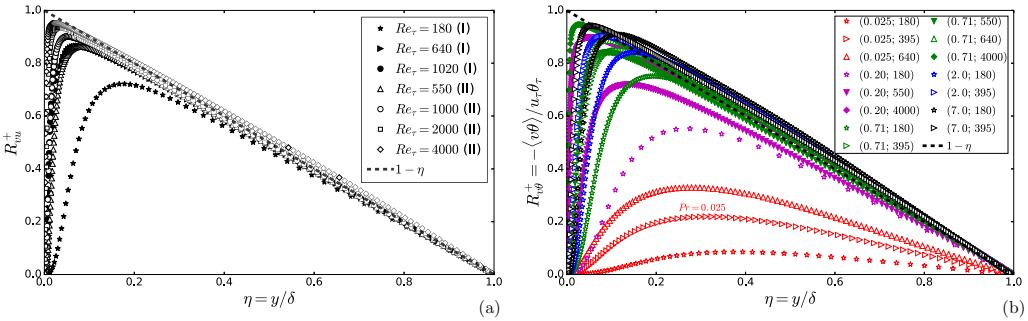

FIG. 2. (a) Outer scaling of the wall-normal turbulent transport of streamwise momentum R^+_{vu} versus η. (b) Outer scaling of the wall-normal turbulent transport of heat $R^+_{v\theta}$ versus η. The legend lists the Prandtl and Reynolds numbers of the data as (Pr; Re_τ). The dashed black line represents $(1-\eta)$. DNS data I are from Kawamura's group [2,6–8,11], and DNS data II are from Ref. [13].

In the outer layer of turbulent channel flow at large Reynolds number and Péclet number, the second term in Eqs. (14a) and (14b) is smaller than the other terms, due to the presence of a prefactor $[1/\mathrm{Re}_\tau] \ll 1$ or $[1/\mathrm{Pe}_\tau] \ll 1$. Thus in the outer layer of turbulent channel flow at high Re_τ and Pe_τ, Eqs. (14a) and (14b) can be approximated as

$$0 \approx 1 + \frac{\partial R^+_{vu}}{\partial \eta}; \quad 0 \approx \frac{U^+}{U^+_b} + \frac{\partial R^+_{v\theta}}{\partial \eta}. \tag{15}$$

Moreover in the outer region of turbulent channel flow at sufficient high Reynolds number, $U^+ \approx U^+_b$, so the MHB equation can be further approximated as

$$0 \approx 1 + \frac{\partial R^+_{v\theta}}{\partial \eta}. \tag{16}$$

Integrating the approximate Eq. (15a) and the approximate Eq. (16) along the wall-normal direction produces approximations for R^+_{vu} and $R^+_{v\theta}$ *in the outer layer* at sufficiently high Reynolds number and Péclet number as

$$R^+_{vu}(\eta) \approx 1 - \eta; \quad R^+_{v\theta}(\eta) \approx 1 - \eta. \tag{17}$$

In Fig. 2(a) a straight line $(1-\eta)$ is plotted, and it agrees reasonable well with R^+_{vu} in the outer layer of turbulent channel flow at sufficiently high Reynolds number. The variation in Fig. 2(b) reflects the effect of Prandtl numbers. At a low Péclet number, such as $\mathrm{Re}_\tau = 180$ and $\mathrm{Pr} = 0.025$, heat transfer is more laminar-like than turbulent-like. Therefore, $R^+_{v\theta}$ should deviate from the $(1-\eta)$ approximation, which is valid for high Péclet numbers. Excluding the low Péclet number data ($\mathrm{Pr} = 0.025$, colored red in the figure), Fig. 2(b) shows that the $R_{v\theta}$ data are better approximated by the $(1-\eta)$ curve. In short, Fig. 2 shows that R^+_{vu} versus η and $R^+_{v\theta}$ versus η properly scale the wall-normal turbulent transport of momentum and heat in the outer layer at sufficiently high Reynolds number Re_τ and sufficiently high Péclet number Pe_τ.

Equations (17a) and (17b) reveal that $R^+_{vu}(\eta)$ and $R^+_{v\theta}(\eta)$ are bounded by 1, an indicator of proper scaling. As η approaches 0, R^+_{vu} and $R^+_{v\theta}$ would approach 1 according to Eqs. (17a) and (17b). However, dictated by the no-slip boundary conditions, $R^+_{vu}(\eta)$ and $R^+_{v\theta}(\eta)$ must be 0 at the wall. Therefore, within a thin layer adjacent to the wall, R^+_{vu} and $R^+_{v\theta}$ must decrease from their peak values to 0 at the channel wall. In other words, the approximate Eqs. (17a) and (17b) are not applicable in the inner region, and another scaling has to be applied there.

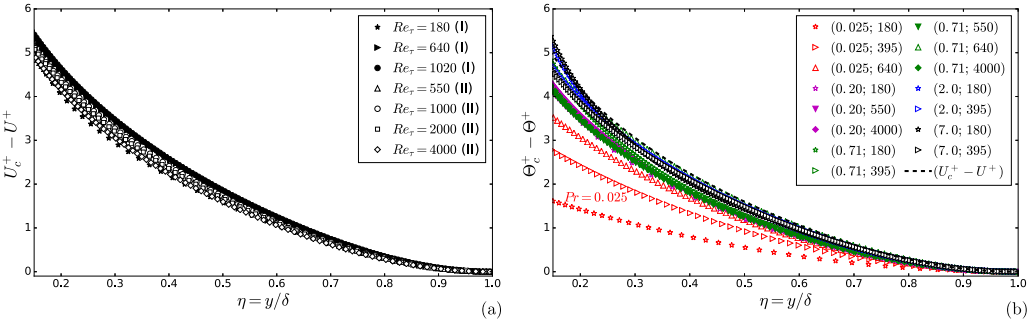

FIG. 3. (a) Traditional outer scaling of the mean streamwise velocity deficit. (b) Traditional outer scaling of the mean temperature deficit. The dashed black curve represents $(U_c^+ - U^+)$ at $\mathrm{Re}_\tau = 4000$.

2. *Traditional outer scaling of the mean velocity and temperature deficit*

In Fig. 3 we evaluate the appropriateness of outer-scaled Eq. (14) by plotting the profiles of mean velocity and mean temperature in the outer layer. Traditionally, the mean velocity and the mean temperature in the outer region are presented as the deficit from their centerline values:

$$\frac{U_c - U}{u_\tau} = U_c^+ - U^+; \quad \frac{\Theta_c - \Theta}{\theta_\tau} = \Theta_c^+ - \Theta^+. \tag{18}$$

An obvious advantage of the deficit profile is that it forces a data collapse at the channel centerline $\eta = 1$ with a zero deficit.

Figure 3(a) shows reasonable collapse of the mean velocity deficit profiles from different Reynolds numbers. In comparison, Fig. 3(b) shows more variation in the scaled mean temperature deficit profiles, especially at low Prandtl number and Reynolds number. The variations can be attributed to, first, low Reynolds number effect, specifically at $\mathrm{Re}_\tau = 180$; second, low Péclet number effect, as in the case at $\mathrm{Re}_\tau = 640$ and $\mathrm{Pr} = 0.025$, and the Reynolds number of this case is large enough, but the Péclet number is small at $\mathrm{Pe}_\tau = 16$; and, third, a deficiency of the traditional scaling.

Next we will present an alternative scaling for the mean temperature deficit and the mean velocity deficit in the outer layer.

3. *Alternative outer scaling of the mean temperature deficit and mean velocity deficit*

In studying turbulent pipe flows and flat-plate turbulent boundary layer flows, Zagarola and Smits found that the mean velocity deficit profiles $(U_c - U)$ in the outer layer collapse better if scaled by $(\delta_{1m}/\delta)U_c$ than if scaled by u_τ as in the traditional scaling [31]. Here δ_{1m} denotes the mass displacement thickness defined as

$$\delta_{1m} \equiv \int_0^\delta \left[1 - \frac{U(y)}{U_c}\right] dy = \frac{U_c - U_b}{U_c}\delta. \tag{19}$$

Similarly, a thermal displacement thickness $\delta_{1\theta}$ can be defined as

$$\delta_{1\theta} \equiv \int_0^\delta \left[1 - \frac{\Theta(y)U(y)}{\Theta_c U_b}\right] dy = \frac{\Theta_c - \Theta_m}{\Theta_c}\delta. \tag{20}$$

Wang *et al.* have applied a Zagarola-Smits-style scaling for the mean temperature distribution within turbulent boundary layer flows [24]. Their definition of the thermal displacement thickness is $\int_0^\delta \frac{T - T_\infty}{T_w - T_\infty} dy$.

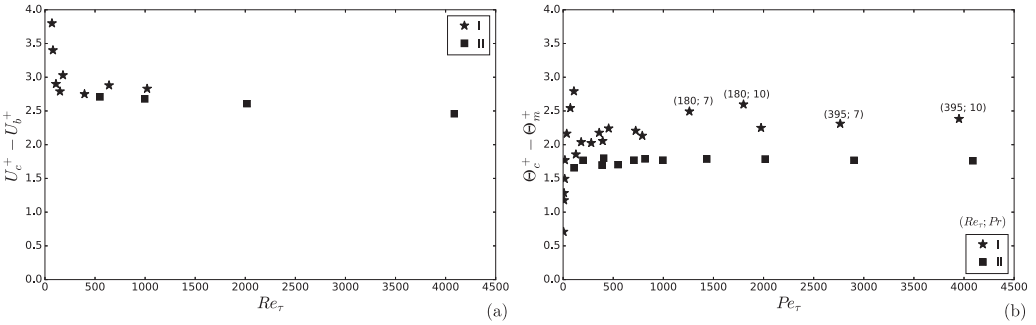

FIG. 4. (a) $(U_c^+ - U_b^+)$ versus Reynolds number. Note that if a logarithmic function is used to approximate U^+, $(U_c^+ - U_b^+) \approx 1/\kappa \approx 2.5$. (b) $(\Theta_c^+ - \Theta_m^+)$ versus Pe_τ. DNS data from Kawamura's group cover Reynolds numbers of $\mathrm{Re}_\tau = 180$, 395, 640, 1020, and Prandtl numbers of $\mathrm{Pr} = 0.025$ to 10 [2,6–8,11]. PBO data include Reynolds numbers of $\mathrm{Re}_\tau = 550$, 1000, 2000, 4000 and Prandtl numbers of $\mathrm{Pr} = 0.2$, 0.71, 1.0 [13].

Using the definitions in Eqs. (19) and (20), the Zagarola-Smits-style scaling for the mean velocity and the mean temperature can be expressed as

$$U_{\mathrm{ZS}} = \frac{\delta_{1m}}{\delta} U_c = \left(\frac{\delta_{1m}}{\delta} U_c^+\right) u_\tau = (U_c^+ - U_b^+) u_\tau, \tag{21}$$

$$\Theta_{\mathrm{ZS}} = \frac{\delta_{1\theta}}{\delta} \Theta_c = \left(\frac{\delta_{1\theta}}{\delta} \Theta_c^+\right) \theta_\tau = (\Theta_c^+ - \Theta_m^+) \theta_\tau. \tag{22}$$

When the Zagarola-Smits-style velocity scale is presented as $U_{\mathrm{ZS}} = (\delta_{1m}/\delta) U_c$, it is not clear whether U_{ZS} is an outer velocity scale, an inner velocity scale, or a mixed velocity scale. U_c is an outer velocity scale, but δ_{1m}/δ is a small number that decreases toward 0 at an infinite Reynolds number, as shown in Ref. [32].

In Eqs. (21) and (22) we show that the ZS scale can also be presented as a product of $(U_c^+ - U_b^+)$ and the inner velocity scale u_τ, or as a product of $(\Theta_c^+ - \Theta_m^+)$ and the friction temperature θ_τ. In other words, U_{ZS} and Θ_{ZS} are the traditional inner scale of u_τ and θ_τ multiplied by a weight function. By determining the Reynolds number and the Péclet number dependence of the weight function, we can then compare the ZS scale with the traditional scale.

Figure 4(a) shows that $(U_c^+ - U_b^+)$ approaches a constant value at sufficiently high Reynolds number. It is known that at high Reynolds number, the mean velocity profile U^+ can be reasonably approximated by a logarithmic function, except in the near-wall region [19]. However, this near-wall region becomes a negligible fraction of the channel height at high Re_τ. Approximating U^+ by a logarithmic function, it can be easily shown that at sufficiently high Reynolds number $(U_c^+ - U_b^+) \approx 1/\kappa \approx 2.5$ where κ is the von Kármán constant. Figure 4(a) shows that the constant value at high Reynolds number is indeed close to be 2.5. Therefore at high Reynolds number, U_{ZS} is equivalent to the traditional inner velocity scale u_τ, differing by a numerical factor of about 2.5.

Figure 4(b) shows that $(\Theta_c^+ - \Theta_m^+)$ also approaches a constant value at sufficiently high Péclet number. Thus Θ_{ZS} is equivalent to the traditional inner temperature scale θ_τ at high Péclet number. Comparing data from Kawamura's group [2,6–8,11] and PBO [13], the larger Prandtl number data from Kawamura's group have larger values of $(\Theta_c^+ - \Theta_m^+)$. However, as Reynolds number increases, the difference becomes smaller. In the following we will show that deviation at large Prandtl number is related to the thickness of the molecular thermal diffusion layer.

The mean temperature deficit and the mean velocity deficit scaled by the Zagarola-Smits scale can be written as

$$U^{*\mathrm{ZS}} = \frac{U_c - U}{U_{\mathrm{ZS}}} = \frac{U_c^+ - U^+}{U_c^+ - U_b^+}; \quad \Theta^{*\mathrm{ZS}} = \frac{\Theta_c - \Theta}{\Theta_{\mathrm{ZS}}} = \frac{\Theta_c^+ - \Theta^+}{\Theta_c^+ - \Theta_m^+}. \tag{23}$$

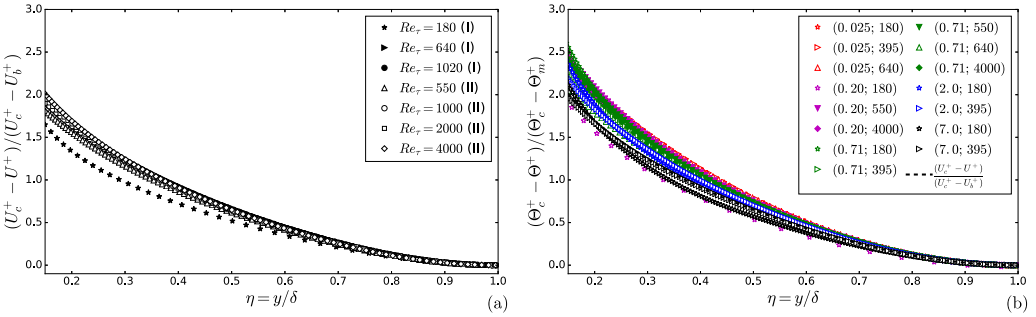

FIG. 5. (a) Zagarola-Smits-style scaled mean streamwise velocity deficit. (b) Zagarola-Smits-style scaled mean temperature deficit. The dashed black curve represents $(U_c^+ - U^+)/(U_c^+ - U_b^+)$ at $\mathrm{Re}_\tau = 4000$.

Using the Zagarola-Smits-style scaling, the MMB equation and the MHB equation become

$$0 = 1 - \left(\frac{U_c^+ - U_b^+}{\mathrm{Re}_\tau}\right)\frac{\partial^2 U^{*\mathrm{ZS}}}{\partial \eta^2} + \frac{\partial R_{vu}^+}{\partial \eta}; \quad 0 = \frac{U^+}{U_b^+} - \left(\frac{\Theta_c^+ - \Theta_m^+}{\mathrm{Pe}_\tau}\right)\frac{\partial^2 \Theta^{*\mathrm{ZS}}}{\partial \eta^2} + \frac{\partial R_{v\theta}^+}{\partial \eta}. \quad (24)$$

Mathematically the outer-scaled Eq. (24) using the ZS scale is equivalent to the traditional outer-scaled Eq. (14). The transformation between Eqs. (24) and (14) is most easily accomplished using the following differentials:

$$dU^{*\mathrm{ZS}} = -\frac{1}{U_c^+ - U_b^+}dU^+; \quad d\Theta^{*\mathrm{ZS}} = -\frac{1}{\Theta_c^+ - \Theta_m^+}d\Theta^+. \quad (25)$$

Replacing dU^+ or $d\Theta^+$ in Eq. (14) with $dU^{*\mathrm{ZS}}$ or $d\Theta^{*\mathrm{ZS}}$, the prefactor of the second term in Eq. (14) is multiplied by $(U_c^+ - U_b^+)$ or $(\Theta_c^+ - \Theta_m^+)$ to produce Eq. (24). As shown in Fig. 4, both $(U_c^+ - U_b^+)$ and $(\Theta_c^+ - \Theta_m^+)$ are bounded and approach a constant value of $O(1)$ at sufficiently high Reynolds number and Péclet number. Therefore, the alternative outer scaling Eq. (24) using ZS scaling is as valid as the traditional outer scaling.

In Fig. 5 we present the mean velocity deficit and the mean temperature deficit scaled by Zagarola-Smits-style scaling. Compared with the traditional scaling in Fig. 3, the ZS scaled mean velocity deficit collapse better, especially for data at low to moderate Reynolds number and Péclet number. Compared with the Zagarola-Smits-style scaled mean velocity deficit in Fig. 5(a), the Zagarola-Smits-style scaled mean temperature displays more variation in Fig. 5(b). The variation again reflects the effect of Péclet numbers. For example, at $\mathrm{Re}_\tau = 180$ and $\mathrm{Pr} = 0.025$, the Péclet number is so low that the heat transfer is more laminar-like than turbulent-like. Consequently the Zagarola-Smits-style scaled mean temperature at these low Péclet numbers should systematically deviate from the data at higher Péclet numbers.

In short, the better collapse of data in the outer layer of Fig. 5 indicates that the ZS scaling, specifically the weight functions $(U_c^+ - U_b^+)$ and $(\Theta_c^+ - \Theta_m^+)$, capture, to a certain degree, the low Reynolds number and low Péclet number effects.

B. Scaling in the "log layer"

It has long been observed that in high Reynolds number turbulent wall-bounded flows there exists a region in which the mean velocity profile can be approximated by a logarithmic function [18–20]. The log law is generally presented using the inner-scaled wall-normal distance $y^+ = y/(\nu/u_\tau)$ and the inner-scaled mean streamwise velocity $U^+ = U/u_\tau$ as

$$U^+ \approx \frac{1}{\kappa}\ln(y^+) + B, \quad (26)$$

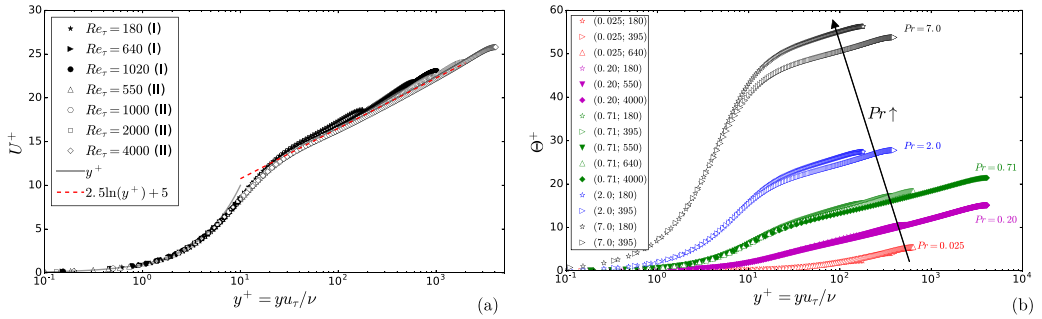

FIG. 6. (a) Traditional inner-scaled mean streamwise velocity versus inner-scaled wall-normal distance, U^+ versus y^+. (b) Traditional inner-scaled mean temperature versus inner-scaled wall-normal distance, Θ^+ versus y^+.

where B is an additive constant. The existence of the "log layer" and the universality of κ have been discussed comprehensively by Nagib and Chauhan [33]. In this work we do not argue for or against the existence of an exact "log law." We regard the logarithmic Eq. (26) as a good approximate function for the mean velocity profile.

To reflect the "log law," the wall-normal distance is scaled as y^+ and the corresponding inner-scaled MMB equation is

$$0 = \frac{1}{\mathrm{Re}_\tau} + \frac{\partial^2 U^+}{\partial y^{+2}} + \frac{\partial R^+_{vu}}{\partial y^+}. \tag{27}$$

Figures 6(a) and 7(a) show the profiles of the inner-scaled U^+ and R^+_{vu} versus y^+. Data from different Reynolds numbers collapse well in the inner region, indicating the appropriateness of the scaling in Eq. (27).

According to Kader and Yaglom, the "log law" for mean temperature was first obtained by Landau and Lifshitz [34]. Applying the classical Izakson-Millikan overlap method [35,36], Kader and Yaglom derived the log law for mean temperature [37]. Recent high Reynolds number DNS [13] has confirmed that the mean scalar field obeys a generalized logarithmic law. Using the traditional inner-scaled wall-normal distance and the inner-scaled mean temperature Θ^+, the log law for mean temperature is commonly presented as

$$\Theta^+ \approx \frac{1}{\kappa_\theta}\ln(y^+) + \beta_\theta(\mathrm{Pr}), \tag{28}$$

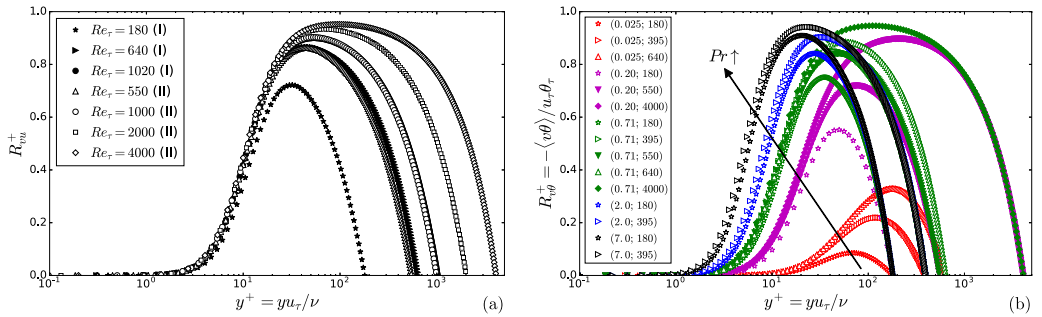

FIG. 7. (a) Traditional inner-scaled turbulent wall-normal transport of streamwise momentum R^+_{vu} versus y^+. (b) Traditional inner-scaled turbulent wall-normal transport of heat $R^+_{v\theta}$ versus y^+.

TABLE I. Additive constant $\beta_\theta(\mathrm{Pr})$ in the thermal log law proposed by previous researchers.

Researcher(s)	$\beta_\theta(\mathrm{Pr})$
Squire (1951) [30]	$\ln[(5\mathrm{Pr}+1)/30)]+8.55+5\mathrm{Pr}$
Levich (1962) [39]	$\alpha_\theta \ln(\mathrm{Pr})+\mathrm{const}$
Gowen and Smith (1967) [40]	$\ln[(5\mathrm{Pr}+1)/30)]+8.55\mathrm{Pr}_t+5\mathrm{Pr}$
Neumann (1968) [41]	$3.5\mathrm{Pr}$
Fortier (1968) [42]	$2.5\ln(\mathrm{Pr})+2.7\mathrm{Pr}-1$
Kader and Yaglom (1972) [37]	$2.12\ln(\mathrm{Pr})+(12.5\mathrm{Pr}^{2/3}-5.3)$ for $\mathrm{Pr}\gtrsim 0.7$ (KA-28)
	$2.12\ln(\mathrm{Pr})+(12.5\mathrm{Pr}^{2/3}-1.5)$ for $\mathrm{Pr}\ll 1$ (KA-31)
Kader (1981) [38]	$2.12\ln(\mathrm{Pr})+(14.8\mathrm{Pr}^{2/3}-10\mathrm{Pr}^{1/3}+1.69)$
Kays and Crawford (1993) [43]	$13.39\mathrm{Pr}^{2/3}-5.66$

where κ_θ is the counterpart of the von Kárman constant. Kader suggested a valued of $\kappa_\theta \approx 1/2.12$ based on a wide range of experimental data [38] (Kader used the notation of $\alpha_\theta = 1/\kappa_\theta = 2.12$). The additive constant β_θ strongly depends on the Prandtl number, and different forms have been proposed in the past, as listed in Table I.

The inner-scaled mean MHB equation corresponding to the traditional thermal log law, using y^+ and Θ^+, reads

$$0=\frac{1}{\mathrm{Re}_\tau}\frac{U^+}{U_b^+}+\frac{1}{\mathrm{Pr}}\frac{\partial^2\Theta^+}{\partial y^{+2}}+\frac{\partial R_{v\theta}^+}{\partial y^+}. \tag{29}$$

The traditional inner-scaled mean temperature Θ^+ and turbulent wall-normal turbulent transport of heat $R_{v\theta}^+$ from different Reynolds number and Prandtl number do not collapse in the inner region, as shown in Figs. 6(b) and 7(b). This is not surprising because, formally, the traditional inner-scaled MHB Eq. (29) is not an analogy of the inner-scaled MMB Eq. (27), due to the presence of a prefactor $1/\mathrm{Pr}$ in front of the second term in the MHB Eq. (29).

Next we present an alternative inner scaling to better represent the "log layer" for the MHB equation. The objective of the alternative scaling is to make the scaled MHB equation formally analogous to the inner-scaled MMB Eq. (27). This can be achieved at least in three ways: (1) rescale the mean temperature only, (2) rescale the wall-normal distance only, and (3) rescale both the mean temperature and the wall-normal distance.

1. Alternative inner scaling for the mean thermal energy equation: Rescale distance

Analogous to the definition of inner-length scale for momentum transfer, a thermal inner length scale can be defined as

$$l_\alpha \equiv \frac{\alpha}{u_\tau}, \tag{30}$$

and a thermal inner-scaled wall-normal distance can then be defined as

$$y^{+_\theta} \equiv \frac{y}{l_\alpha}=\frac{y}{\alpha/u_\tau}=y^+\mathrm{Pr}. \tag{31}$$

Hence an alternative inner scaling of the MHB equation can be expressed as

$$0=\frac{1}{\mathrm{Pe}_\tau}\frac{U^+}{U_b^+}+\frac{\partial^2\Theta^+}{\partial y^{+_\theta 2}}+\frac{\partial R_{v\theta}^+}{\partial y^{+_\theta}}, \tag{32}$$

where the Péclet number is defined as $\mathrm{Pe}_\tau = \mathrm{Re}_\tau\mathrm{Pr}$. Note that the scaling for $R_{v\theta}^+$ itself remains the same, but its gradient in the wall-normal direction is modified through y^{+_θ}. Formally, the Pe_τ in the MHB Eq. (32) is the counterpart of Re_τ in the MMB Eq. (27).

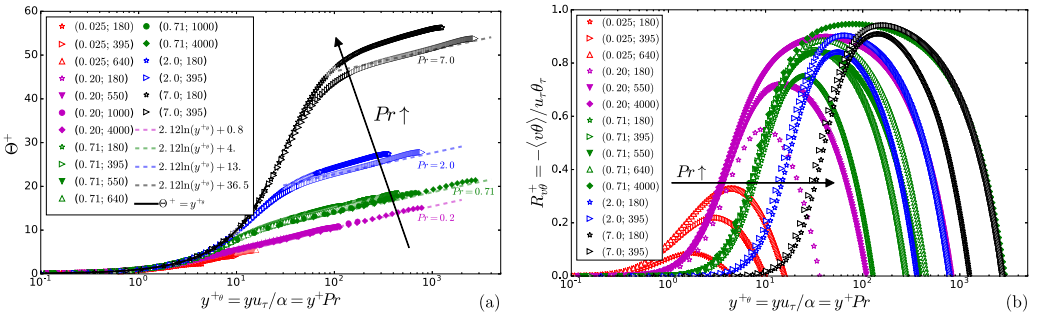

FIG. 8. Alternative inner scaling for the mean thermal energy equation by rescaling the wall-normal distance as $y^{+\theta} = y^+\mathrm{Pr}$. (a) Mean temperature. Dashed lines represent the log law at different Prandtl numbers. The solid black line represents the linear behavior in the molecular diffusion sublayer. (b) Turbulent wall-normal transport of heat.

In Fig. 8 we present the inner-scaled mean temperature and wall-normal turbulent transport of heat versus the alternative inner-scaled wall-normal distance $y^{+\theta}$. A salient property of $y^{+\theta} = y^+\mathrm{Pr}$ is that the slope of the "log layer" from different Prandtl numbers is roughly the same, indicated by the dashed lines with the same slope in Fig. 8(a). The effect of Prandtl numbers is to shift the end of the molecular thermal diffusion sublayer and buffer layer to larger $y^{+\theta}$ with increasing Pr. Figure 8(b) shows that the profiles of $R^+_{v\theta}$ from different Péclet numbers display a similar shape with respect to $y^{+\theta}$ at sufficiently high Péclet numbers. As the Péclet number increases, the $R^+_{v\theta}$ peak value increases and approaches a value of 1. At the same time, the $R^+_{v\theta}$ peak location moves outward as the Péclet number increases.

A log law consistent with the alternative inner-scaled MHB Eq. (32), using $y^{+\theta}$ instead of y^+, reads

$$\Theta^+ \approx \frac{1}{\kappa_\theta}\ln(y^{+\theta}) + B_\theta(\mathrm{Pr}) = \frac{1}{\kappa_\theta}\ln(\mathrm{Pr}y^+) + B_\theta(\mathrm{Pr}). \tag{33}$$

Note that the additive constant $B_\theta(\mathrm{Pr}) = \beta_\theta(\mathrm{Pr}) - \frac{1}{\kappa_\theta}\ln(\mathrm{Pr})$.

Figure 8 shows that $y^{+\theta}$ is a good choice to present the "log layer." However, the molecular thermal diffusion sublayer and buffer layer require scaling different from $y^{+\theta}$, which is addressed in the following section.

C. Scaling in the molecular diffusion sublayer

It is well known that, within a thin layer adjacent to the channel wall, the increase of the mean temperature with wall-normal distance can be approximated by a linear function [38]. A common way to present the linear profile in the literature is by rescaling the mean temperature as

$$\Theta^{+_\theta} = \frac{\Theta}{\theta_\tau \mathrm{Pr}} = \frac{\Theta^+}{\mathrm{Pr}}. \tag{34}$$

Plotting Θ^{+_θ} versus the traditionally inner-scaled wall-normal distance y^+, the near-wall region can be approximated by a straight line, as shown in Fig. 9(a). Using Θ^{+_θ}, an alternative inner-scaled MHB equation can be written as

$$0 = \frac{1}{\mathrm{Re}_\tau}\frac{U^+}{U_b^+} + \frac{\partial^2\Theta^{+_\theta}}{\partial y^{+2}} + \frac{\partial R^+_{v\theta}}{\partial y^+}. \tag{35}$$

Nominally this inner-scaled MHB equation is analogous to the inner-scaled MMB Eq. (27). Note that in this alternative inner scaling, the wall-normal turbulent transport of heat is not affected, and Péclet number does not appear in the equation.

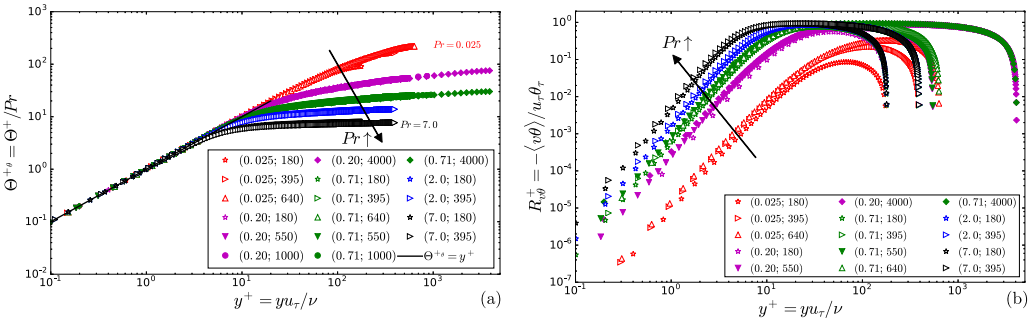

FIG. 9. (a) Rescaled mean temperature as $\Theta^{+\theta} = \frac{\Theta^+}{\mathrm{Pr}}$ versus y^+. The solid black line represents the linear function. (b) Inner-scaled wall-normal turbulent transport of heat $R^+_{v\theta}$ versus y^+.

To evaluate the validity of this rescaling, Fig. 9(a) presents profiles of $\Theta^{+\theta} = \Theta^+/\mathrm{Pr}$ versus y^+ on loglog axes, to better show the near-wall region. Figure 9(a) clearly shows that the rescaled mean temperature from different Re_τ and Pr collapses well onto a straight line for small y^+, but the slopes of the rescaled mean temperature profiles are different outside the "linear region." In other words, $\Theta^{+\theta}$ versus y^+ is not a good way to represent the log law of the mean temperature.

Figure 9(b) shows that the inner-scaled $R^+_{v\theta}$ profiles from different Re_τ and Pr do not collapse in the molecular thermal diffusion sublayer. Moreover, the trend of $R^+_{v\theta}$ in Fig. 9(b) is not as obvious as in Fig. 8(b). Figure 9 indicates that y^+ is not an appropriate scaling in the molecular thermal diffusion sublayer. In short, Eq. (35) is not a good choice of inner scaling for the molecular thermal diffusion sublayer, and presenting Θ^+/Pr versus y^+ should be avoided in the study of turbulent heat transfer, as it does not correspond to a proper scaling of the MHB equation.

In the following we will rescale both Θ and y to better represent the scaling in the molecular thermal diffusion sublayer.

1. Thickness of the molecular diffusion sublayer

In a fully developed turbulent channel flow, there exists a thin layer adjacent to the wall where $U^+ \approx y^+$, as shown in Fig. 6(a). The thickness of this viscous sublayer, or molecular momentum diffusion sublayer, is $y^+ \lesssim 6$ [19]. In other words, the thickness of the molecular momentum diffusion sublayer is

$$y_{l_m} \approx 6\frac{\nu}{u_\tau} \quad \text{or} \quad y^+_{l_m} \approx 6. \tag{36}$$

Similarly, there also exists a molecular thermal diffusion sublayer in which Θ^+ grows linearly with y^+, as shown in Figs. 8(a) and 9(a). However, unlike the momentum transfer case, the thickness of the molecular thermal diffusion sublayer is strongly influenced by the Prandtl number of the fluid.

The thickness of the molecular thermal diffusion sublayer y_{l_t} can be defined in several ways. For example, Kader used an eddy viscosity model for $R_{v\theta}$ and defined the thickness of y_{l_t} by specifying certain properties of the eddy viscosity [38]. One can also define the thickness of y_{l_t} based on the ratio between the diffusion term and the turbulence term in the MHB Eq. (29) or (35) [23]. Here we adopt a simpler and more practical definition based on the deviation of Θ from the linear shape as

$$\frac{\Theta^+ - \mathrm{Pr}y^+}{\Theta^+} \approx -0.05. \tag{37}$$

The 5% is chosen to match the thickness of the viscous sublayer y_{l_m} at $\mathrm{Pr} = 1$. Figure 10 shows that the thickness of the molecular thermal diffusion layer, based on DNS data from Kawamura's group

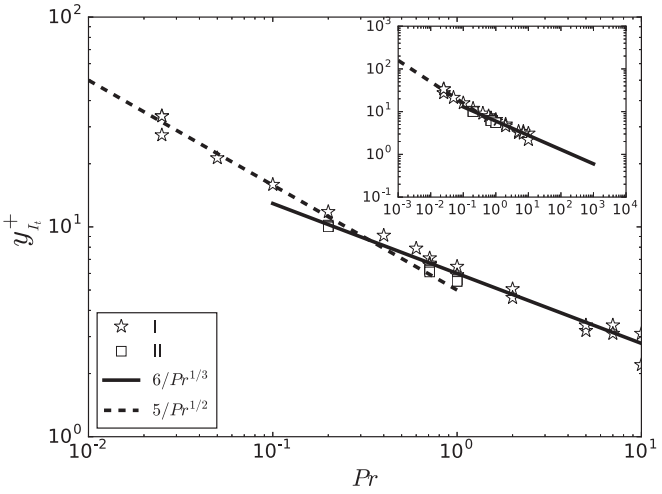

FIG. 10. Thickness of the molecular thermal diffusion sublayer, y_{I_t}.

[2,6–8,11] and PBO [13]. The DNS data indicate that

$$y_{I_t} \approx \left(5\frac{\nu}{u_\tau}\right)\mathrm{Pr}^{-1/2} \quad \text{or} \quad y^+_{I_t} \approx \frac{5}{\mathrm{Pr}^{1/2}} \quad \mathrm{Pr} < O(1), \tag{38}$$

$$y_{I_t} \approx \left(6\frac{\nu}{u_\tau}\right)\mathrm{Pr}^{-1/3} \quad \text{or} \quad y^+_{I_t} \approx \frac{6}{\mathrm{Pr}^{1/3}} \quad \mathrm{Pr} > O(1). \tag{39}$$

Figure 10 shows that the transition between low Prandtl number scaling and high Prandtl number scaling occurs at $\mathrm{Pr} \approx 0.5$, but more data and especially high-resolution DNS data are required to more precisely determine the transition Prandtl number.

At this stage, the Prandtl number dependence of the molecular thermal diffusion sublayer thickness, and specifically the power laws in Eqs. (38) and (39) and the exponents of $-1/2$ and $-1/3$, is empirically driven. The power law Prandtl number dependence can be obtained by a simple dimensional consideration, but a more rigorous physically based derivation of the Prandtl number dependence remains open. Monin and Yaglom comprehensively examined the dependence of conductive sublayer thickness on the Prandtl number [20]. Based on an extensive review of experimental data of mass and heat transfer, in particular data for high Prandtl numbers or Schmidt numbers, Monin and Yaglom concluded that the exponent of the Prandtl number dependence is about $-1/3$ [20]. However, subtle differences between the Prandtl number dependence at low Prandtl numbers and high Prandtl numbers have been reported by researchers, and an exponent of $-1/2$ has been suggested for low Prandtl numbers [38,44–47].

Equations (38) and (39) show that the thickness of the molecular thermal diffusion sublayer is strongly influenced by the Prandtl number. Therefore, scaling of the wall-normal distance in the molecular thermal diffusion sublayer must incorporate the Prandtl number of the fluid. In the following, we present a general way of rescaling the wall-normal distance, and the accompanying rescaling of the mean temperature.

2. Alternative inner scaling: Rescale both Θ and y

A general way of presenting the rescaled Θ and y is using differentials [14,15]:

$$dy^* = \mathrm{Pr}^b dy^+; \quad d\Theta^* = \mathrm{Pr}^a d\Theta^+. \tag{40}$$

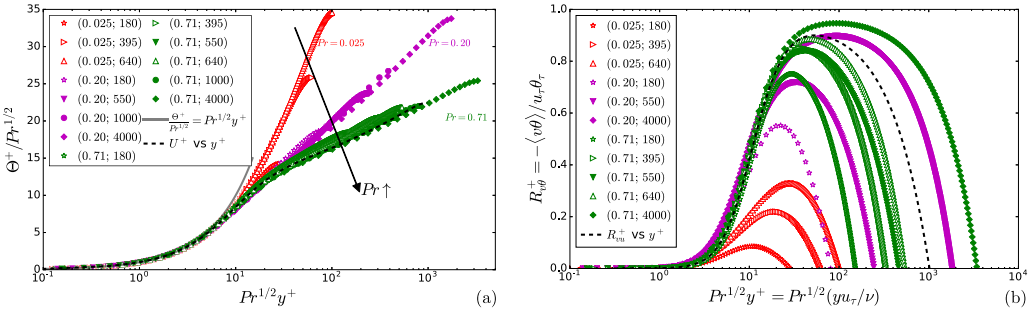

FIG. 11. Scaling of the molecular thermal diffusion and buffer layer at small Prandtl number $\mathrm{Pr} < 1$. (a) Mean temperature $\Theta^+/\mathrm{Pr}^{1/2}$ versus $\mathrm{Pr}^{1/2}y^+$. The solid gray line indicates linear behavior. The dashed black line represents the mean velocity profile at $\mathrm{Re}_\tau = 1000$. (b) Wall-normal turbulent transport of heat $R^+_{v\theta}$ versus $\mathrm{Pr}^{1/2}y^+$. The dashed black line represents the Reynolds shear stress at $\mathrm{Re}_\tau = 1000$.

The rescaled MHB equation becomes

$$0 = \frac{1}{\mathrm{Re}_\tau}\frac{U^+}{U_b^+} + \left(\frac{1}{\mathrm{Pr}}\frac{\mathrm{Pr}^{-a}}{\mathrm{Pr}^{-2b}}\right)\frac{\partial^2\Theta^*}{\partial y^{*2}} + \frac{1}{\mathrm{Pr}^{-b}}\frac{\partial R^+_{v\theta}}{\partial y^*}. \tag{41}$$

Multiplying the equation by Pr^{-b} produces

$$0 = \left(\frac{1}{\mathrm{Re}_\tau \mathrm{Pr}^b}\right)\frac{U^+}{U_b^+} + \left(\frac{1}{\mathrm{Pr}^{1+a-b}}\right)\frac{\partial^2\Theta^*}{\partial y^{*2}} + \frac{\partial R^+_{v\theta}}{\partial y^*}. \tag{42}$$

To make Eq. (42) formally analogous to the inner-scaled MMB Eq. (27), the prefactor in front of the second term has to be 1:

$$a = b - 1. \tag{43}$$

Therefore, an alternative inner-scaled mean thermal energy equation can be written as

$$0 = \left(\frac{1}{\mathrm{Re}_\tau \mathrm{Pr}^b}\right)\frac{U^+}{U_b^+} + \frac{\partial^2(\mathrm{Pr}^{b-1}\Theta^+)}{\partial(\mathrm{Pr}^b y^+)^2} + \frac{\partial R^+_{v\theta}}{\partial(\mathrm{Pr}^b y^+)}. \tag{44}$$

The rescaling of the wall-normal distance as $y^+\mathrm{Pr}^b$ has been employed by Saha and colleagues [21,22]. One implication of Eq. (44) is that for the scaling of the molecular thermal diffusion sublayer, the relevant Péclet number is $\mathrm{Re}_\tau\mathrm{Pr}^b$, not $\mathrm{Pe}_\tau = \mathrm{Re}_\tau\mathrm{Pr}$.

3. Scaling of the molecular thermal diffusion sublayer for Pr ≪ 1

For low Prandtl number, the molecular thermal diffusion sublayer thickness is $y^+_{l_t} \approx 5/\mathrm{Pr}^{1/2}$ or $b = 1/2$, as shown in Sec. III C 1. Hence a proper rescaling of the wall-normal distance y is $y^+\mathrm{Pr}^{1/2}$, and the corresponding inner-scaled mean temperature is $\Theta^+/\mathrm{Pr}^{1/2}$. The alternative inner-scaled MHB equation for the molecular thermal diffusion sublayer at low Pr becomes

$$0 = \left(\frac{1}{\mathrm{Re}_\tau \mathrm{Pr}^{1/2}}\right)\frac{U^+}{U_b^+} + \frac{\partial^2(\Theta^+/\mathrm{Pr}^{1/2})}{\partial(\mathrm{Pr}^{1/2}y^+)^2} + \frac{\partial R^+_{v\theta}}{\partial(\mathrm{Pr}^{1/2}y^+)}. \tag{45}$$

Figure 11(a) presents the rescaled mean temperature $\Theta^+/\mathrm{Pr}^{1/2}$ versus $\mathrm{Pr}^{1/2}y^+$ from DNS data at low Prandtl numbers, showing good agreement in the molecular thermal diffusion sublayer and

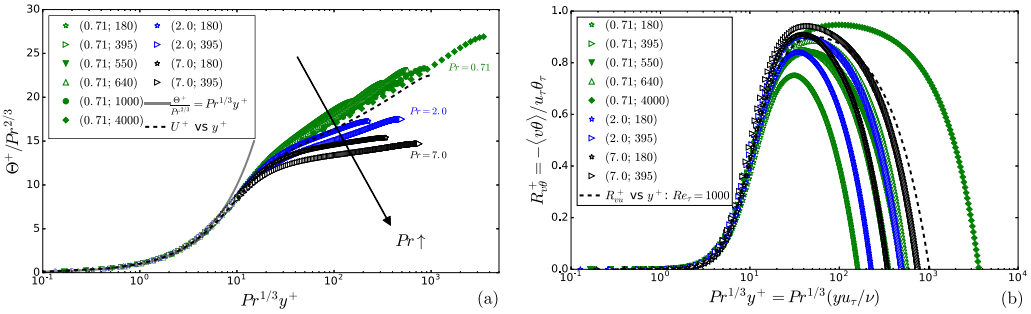

FIG. 12. Scaling of the molecular thermal diffusion sublayer and buffer layer at large Prandtl number Pr > 1. (a) Mean temperature $\Theta^+/\mathrm{Pr}^{2/3}$ versus $\mathrm{Pr}^{1/3}y^+$. Solid curve represents the linear profile, and the dashed curve is mean velocity profile U^+ versus y^+. (b) Wall-normal turbulent transport of heat $R^+_{v\theta}$ versus $\mathrm{Pr}^{1/3}y^+$. Dashed curve is R^+_{vu} versus y^+.

buffer layer. Figure 11(b) also shows good collapse of $R^+_{v\theta}$ versus $\mathrm{Pr}^{1/2}y^+$ in the molecular thermal diffusion sublayer and buffer layer. To highlight the similarity between the MHB equation and the MMB equation, one U^+ profile is plotted versus y^+ in Fig. 11(a), and one R^+_{vu} profile is plotted versus y^+ in Fig. 11(b). Figure 11 displays a striking similarity, when properly scaled, between the mean velocity or Reynolds shear stress and the mean temperature or turbulent transport of heat within the molecular diffusion sublayer.

4. Scaling of the molecular thermal diffusion sublayer for $Pr \gg 1$

At high Prandtl number, the molecular thermal diffusion sublayer thickness is $y^+ \approx 6/\mathrm{Pr}^{1/3}$ or $b = 1/3$, as shown in Sec. III C 1. Thus a proper rescaling of y is $y^+\mathrm{Pr}^{1/3}$, the corresponding inner-scaled mean temperature is $\Theta^+/\mathrm{Pr}^{2/3}$, and the alternative inner-scaled equation is

$$0 = \left(\frac{1}{\mathrm{Re}_\tau \mathrm{Pr}^{1/3}}\right)\frac{U^+}{U_b^+} + \frac{\partial^2(\Theta^+/\mathrm{Pr}^{2/3})}{\partial(\mathrm{Pr}^{1/3}y^+)^2} + \frac{\partial R^+_{v\theta}}{\partial(\mathrm{Pr}^{1/3}y^+)}. \tag{46}$$

Figure 12(a) shows the scaled mean temperature $\Theta^+/\mathrm{Pr}^{2/3}$ versus $\mathrm{Pr}^{1/3}y^+$. The mean temperature profiles from cases with different Reynolds numbers and Prandtl number $\mathrm{Pr} \geqslant 0.71$ collapse well in the molecular diffusion sublayer and buffer layer. Figure 12(b) shows that $R^+_{v\theta}$ from different Re and Pr also collapse well in the molecular sublayer when plotted against $\mathrm{Pr}^{1/3}y^+$. To highlight the similarity between turbulent heat transfer and flow in the molecular diffusion sublayer, the U^+ profile and R^+_{vu} profile at $\mathrm{Re}_\tau = 1000$ are presented in Fig. 12. Again, when properly scaled, the mean temperature and wall-normal turbulent transport of heat are nearly identical to the mean flow and the Reynolds shear stress within the molecular diffusion sublayer. In short, Fig. 12 supports the validity of the inner-scaled Eq. (46) at large Prandtl number.

At very large Prandtl number, say, $\mathrm{Pr} = 1000$, the molecular thermal diffusion sublayer thickness is $y^+_{l_t} \approx 0.6$, which is deep inside the viscous sublayer. As a result, ultra-fine resolution is required for the numerical simulation of heat transfer at large Prandtl number.

D. Scaling in the mesolayer

The concept of a mesolayer or intermediate layer in turbulent wall-bounded flows has been proposed by a number of researchers, including Long and Chen [48], Afzal [49,50], Sreenivasan [51], Wosnik *et al.* [52], and Wei *et al.* [16]. The mesolayer centers around the peak of R_{vu}, as shown in Fig. 2.

The properties of peak R_{vu} value and location have been experimentally measured and analytically studied. It has long been known that the peak R_{vu} location scales as $y_{mm} \sim \sqrt{\delta\nu/u_\tau}$ or

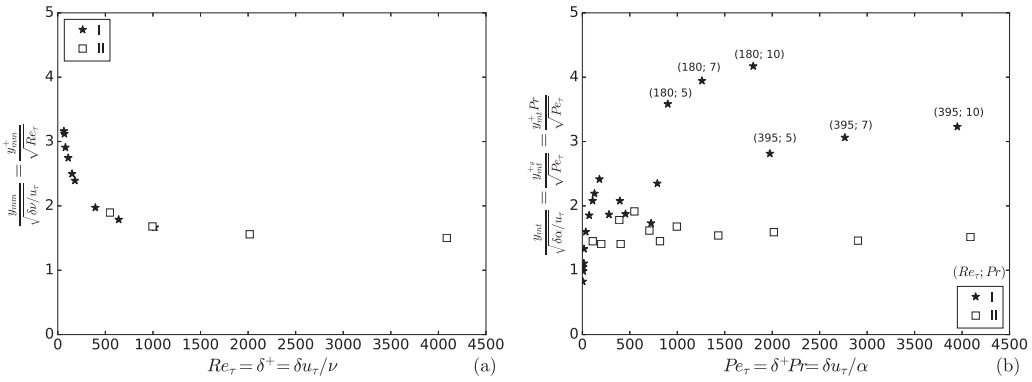

FIG. 13. (a) Peak location of the turbulent wall-normal transport of streamwise momentum, y_{mm}. (b) Peak location of the turbulent wall-normal transport of heat, y_{mt}. DNS from Kawamura's group covers $\mathrm{Re}_\tau = 180$ to 1020 and $\mathrm{Pr} = 0.025$ to $\mathrm{Pr} = 10$. DNS from [13] covers $\mathrm{Re}_\tau = 550$, 1000, 2000, 4000 and $\mathrm{Pr} = 0.2$, 0.71, 1.0.

$y^+_{mm} \sim \sqrt{\mathrm{Re}_\tau}$ [48,49,53]. The peak value of R_{vu} is known to scale as $R^+_{vu,\max} \sim 1 - O(1/\sqrt{\mathrm{Re}_\tau})$. In Fig. 13(a) Reynolds number dependence of the peak R_{vu} location is plotted as $y_{mm}/\sqrt{\delta\nu/u_\tau}$ versus Re_τ. At sufficiently high Reynolds number $\mathrm{Re}_\tau \gtrsim 1000$, Fig. 13(a) shows that the peak R_{vu} location is $y_{mm} \approx 1.5\sqrt{\delta\nu/u_\tau}$. Figure 14(a) presents the Reynolds number dependence of the peak value of R_{vu} as $(1 - R^+_{vu,\max})\sqrt{\mathrm{Re}_\tau}$ versus Re_τ. For $\mathrm{Re}_\tau \gtrsim 1000$, $(1 - R^+_{vu,\max})\sqrt{\mathrm{Re}_\tau} \approx 3.1$.

A thermal mesolayer has also been proposed for the mean thermal energy balance equation [17,26]. Analogous to the momentum mesolayer, the thermal mesolayer centers around the peak of $R_{v\theta}$. To identify proper scaling for the thermal mesolayer, it is essential to determine the properties of the peak $R_{v\theta}$ location and value, and in particular the dependence on Reynolds number, Prandtl number, and Péclet number.

Figure 13(b) presents the Péclet number dependence of the peak $R_{v\theta}$ location y_{mt} by plotting $y_{mt}/\sqrt{\delta\alpha/u_\tau}$ versus Pe_τ. DNS data of PBO in Fig. 13(b) show that, at sufficiently large Reynolds number and Péclet number, the peak $R_{v\theta}$ location y_{mt} location scales as

$$y_{mt} \approx 1.5\sqrt{\frac{\delta\alpha}{u_\tau}}, \quad \text{or} \quad y^+_{mt} \approx 1.5\sqrt{\frac{\mathrm{Re}_\tau}{\mathrm{Pr}}}, \quad \text{or} \quad y^+_{mt} \approx 1.5\sqrt{\mathrm{Re}_\tau \mathrm{Pr}} = 1.5\sqrt{\mathrm{Pe}_\tau}. \tag{47}$$

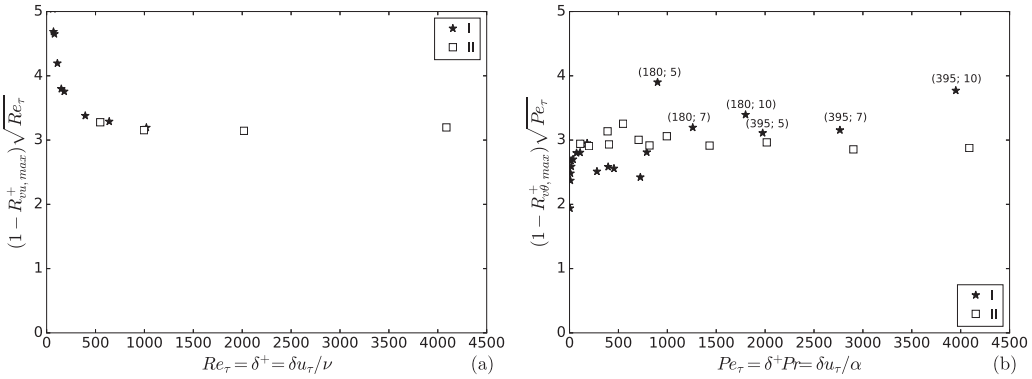

FIG. 14. (a) Peak value of the turbulent wall-normal transport of streamwise momentum, $(1 - R^+_{vu,\max})\sqrt{\mathrm{Re}_\tau}$, versus Reynolds number. (b) Peak value of the turbulent wall-normal transport of heat, $(1 - R^+_{v\theta,\max})\sqrt{\mathrm{Pe}_\tau}$, versus Péclet number.

Figure 13(b) shows that the y_{mt} locations at larger Prandtl number simulations from Kawamura's group have larger values. As discussed above, the thickness of the molecular thermal diffusion sublayer and buffer layer scales as $y_{l_t} \sim O(\frac{1}{\mathrm{Pr}^{1/3}}\frac{\nu}{u_\tau})$ or $y_{l_t}^{+_\theta} \sim O(\mathrm{Pr}^{2/3})$ for large Prandtl number. As a result, the peak $R_{v\theta}$ location $y_{mt}^{+_\theta}$ is shifted outward by $O(\mathrm{Pr}^{2/3})$, as shown in Fig. 13(b). However, as Reynolds number increases, $\sqrt{\mathrm{PrRe}_\tau} \gg \mathrm{Pr}^{2/3}$ and shifting of the molecular thermal diffusion sublayer becomes negligible. For example, at $\mathrm{Pr} = 1000$, the thickness of the molecular thermal diffusion sublayer is $6\mathrm{Pr}^{2/3} = 600$. According to Eq. (47), peak $R_{v\theta}$ location is approximately $1.5\sqrt{\mathrm{Re}_\tau \mathrm{Pr}} = 636$ for $\mathrm{Re}_\tau = 180$. In other words, the outward shifting of the molecular thermal diffusion sublayer is comparable to the scaling in Eq. (47). However, at a very high Reynolds number of $\mathrm{Re}_\tau = 1e5$, $1.5\sqrt{\mathrm{Re}_\tau \mathrm{Pr}} = 15\,000$ becomes much larger than $6\mathrm{Pr}^{2/3} = 600$.

Figure 14(b) presents the Péclet number dependence of the peak $R_{v\theta}$ value by plotting $(1 - R^+_{v\theta,\max})\sqrt{\mathrm{Pe}_\tau}$ versus Pe_τ. DNS data indicate that at sufficiently high Péclet number the peak value of $R_{v\theta}$ scales as

$$1 - R^+_{v\theta,\max} \approx \frac{3.0}{\sqrt{\mathrm{Pe}_\tau}}. \tag{48}$$

The deviation at larger Prandtl number in Fig. 14(b) is again caused by the molecular thermal diffusion sublayer mentioned above.

Scaling relations for the peak $R_{v\theta}$ location and value, Eqs. (47) and (48), are not new. Similar relations have been reported in previous studies, for example, in Refs. [12,23,26,54].

Mesoscaling of the mean thermal energy equation has been proposed by Wei *et al.* [17] and further developed in Refs. [21–23]. Following Fife *et al.* [15,55], we present the mesoscaling of the mean thermal energy equation using differentials

$$dy^{+_\theta} = \alpha_\theta dy^{\Lambda_\theta}, \quad dR^+_{v\theta} = \beta_\theta dR^{\Lambda_\theta}_{v\theta}. \tag{49}$$

Note that α_θ and β_θ in Eq. (49) are not related to the notation in Eq. (28). Substituting the differentials in Eq. (49) into Eq. (32) produces

$$0 = \frac{1}{\mathrm{Pe}_\tau}\frac{U^+}{U_b^+} + \frac{1}{\alpha_\theta^2}\frac{\partial^2\Theta^+}{\partial y^{+_\theta 2}} + \frac{\beta_\theta}{\alpha_\theta}\frac{\partial R^{\Lambda_\theta}_{v\theta}}{\partial y^{+_\theta}}. \tag{50}$$

Matching the formal order of magnitude of each term in Eq. (50) yields [15,55]

$$\frac{1}{\mathrm{Pe}_\tau} = \frac{1}{\alpha_\theta^2}; \quad \frac{1}{\alpha_\theta^2} = \frac{\beta_\theta}{\alpha_\theta}. \tag{51}$$

Thus the parameters α_θ and β_θ in the differentials of Eq. (49) become

$$\alpha_\theta = \sqrt{\mathrm{Pe}_\tau}; \quad \beta_\theta = \frac{1}{\sqrt{\mathrm{Pe}_\tau}}. \tag{52}$$

The mesoscaling of the wall-normal distance and $R_{v\theta}$ is

$$y^{\Lambda_\theta} = \frac{y^{+_\theta} - y^{+_\theta}_{mt}}{\sqrt{\mathrm{Pe}_\tau}}; \quad R^{\Lambda_\theta}_{v\theta} = \sqrt{\mathrm{Pe}_\tau}(R^+_{v\theta} - R^+_{v\theta,\max}). \tag{53}$$

In comparison, the parameters for the mesoscaling of the MMB are [16]

$$\alpha_m = \sqrt{\mathrm{Re}_\tau}, \quad \beta_m = \frac{1}{\sqrt{\mathrm{Re}_\tau}}, \tag{54}$$

$$y^\Lambda = \frac{y^+ - y^+_{mm}}{\sqrt{\mathrm{Re}_\tau}}, \quad R^\Lambda_{vu} = \sqrt{\mathrm{Re}_\tau}(R^+_{vu} - R^+_{vu,\max}). \tag{55}$$

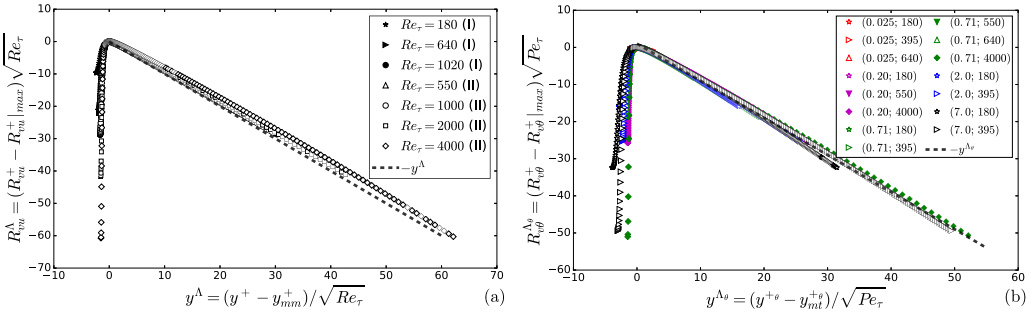

FIG. 15. Mesoscaling of (a) wall-normal turbulent transport of momentum; (b) wall-normal turbulent transport of heat.

The mesoscaled MMB equation and MHB equation can be written as

$$0 = 1 + \frac{\partial^2 U^+}{\partial y^{\Lambda 2}} + \frac{\partial R^\Lambda_{vu}}{\partial y^\Lambda}; \quad 0 = \frac{U^+}{U^+_b} + \frac{\partial^2 \Theta^+}{\partial y^{\Lambda_\theta 2}} + \frac{\partial R^{\Lambda_\theta}_{v\theta}}{\partial y^{\Lambda_\theta}}. \tag{56}$$

By construction, a salient property of the mesoscaling is that the prefactor of each term is 1. Figure 15(a) shows that the mesoscaled R^Λ_{vu} profiles from different Reynolds numbers collapse well around the mesolayer, supporting the appropriateness the mesoscaling Eq. (56). Similarly, the mesoscaled $R^{\Lambda_\theta}_{v\theta}$ profiles from different Reynolds numbers and Prandtl numbers collapses well in Fig. 15(b). This collapse shows that the effect of Prandtl number is represented well by the Péclet number $\mathrm{Pe}_\tau = \mathrm{PrRe}_\tau$ used in Eq. (52).

It is challenging to use the exact mesoscaling in Eq. (53) to present experimental data, as the peak $R_{v\theta}$ data are often not available from experimental measurements. Wei *et al.* [56] introduced an approximate mesoscaling as $\sqrt{\mathrm{Re}_\tau}(R^+_{vu} - 1)$ versus $y^+/\sqrt{\mathrm{Re}_\tau}$. The corresponding approximate thermal mesoscaling is $\sqrt{\mathrm{Pe}_\tau}(R^+_{v\theta} - 1)$ versus $y^{+_\theta}/\sqrt{\mathrm{Pe}_\tau} = (\mathrm{Pr}y^+)/\sqrt{\mathrm{Pe}_\tau}$. As shown in Fig. 16, the approximate mesoscaling collapses the DNS data reasonably well.

In the outer layer the mesoscaling for R_{vu} and $R_{v\theta}$ transitions naturally to outer scaling, due to the following relation:

$$\frac{\partial R^\Lambda_{vu}}{\partial y^\Lambda} = \frac{\frac{1}{\beta_m}}{\frac{1}{\alpha_m}} \frac{\partial R^+_{vu}}{\partial y^+} = \mathrm{Re}_\tau \frac{\partial R^+_{vu}}{\partial y^+} = \frac{\partial R^+_{vu}}{\partial \eta}; \quad \frac{\partial R^{\Lambda_\theta}_{v\theta}}{\partial y^{\Lambda_\theta}} = \frac{\frac{1}{\beta_\theta}}{\frac{1}{\alpha_\theta}} \frac{\partial R^+_{v\theta}}{\partial y^{+_\theta}} = \mathrm{Pe}_\tau \frac{\partial R^+_{v\theta}}{\partial y^{+_\theta}} = \frac{\partial R^+_{v\theta}}{\partial \eta}. \tag{57}$$

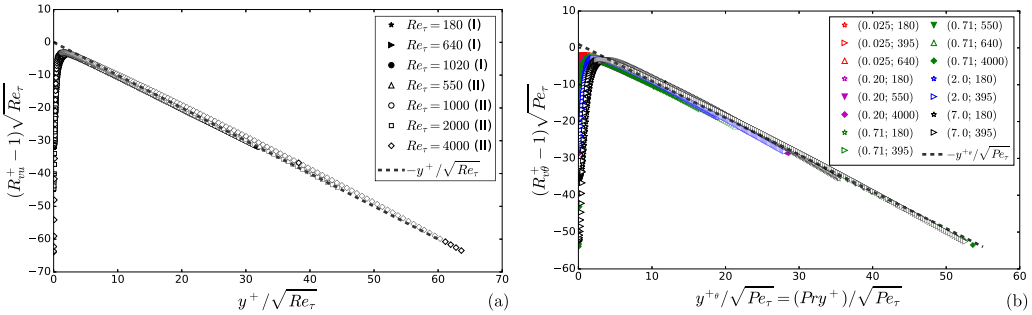

FIG. 16. Approximate mesoscaling of (a) wall-normal turbulent transport of momentum; (b) wall-normal turbulent transport of heat.

TABLE II. Summary of multiscaling of the MHB equation, in comparison with the MMB equation. Note that Zagarola-Smits-style scaling in Eq. (24) is also valid in the outer layer.

	MMB equation	MHB equation
Diffusion sublayer	$0 = \frac{1}{[\mathrm{Re}_\tau]} + \frac{\partial^2 U^+}{\partial y^{+2}} + \frac{\partial R_{vu}^+}{\partial y^+}$	$0 = \frac{1}{\left[\mathrm{Re}_\tau \mathrm{Pr}^{\frac{1}{2}}\right]} \frac{U^+}{U_b^+} + \frac{\partial^2 \left(\Theta^+/\mathrm{Pr}^{\frac{1}{2}}\right)}{\partial \left(\mathrm{Pr}^{\frac{1}{2}} y^+\right)^2} + \frac{\partial R_{v\theta}^+}{\partial \left(\mathrm{Pr}^{\frac{1}{2}} y^+\right)}$: $\mathrm{Pr} < 1$
		$0 = \frac{1}{\left[\mathrm{Re}_\tau \mathrm{Pr}^{\frac{1}{3}}\right]} \frac{U^+}{U_b^+} + \frac{\partial^2 \left(\Theta^+/\mathrm{Pr}^{\frac{1}{3}}\right)}{\partial \left(\mathrm{Pr}^{\frac{1}{3}} y^+\right)^2} + \frac{\partial R_{v\theta}^+}{\partial \left(\mathrm{Pr}^{\frac{1}{3}} y^+\right)}$: $\mathrm{Pr} > 1$
Log layer	$0 = \frac{1}{[\mathrm{Re}_\tau]} + \frac{\partial^2 U^+}{\partial y^{+2}} + \frac{\partial R_{vu}^+}{\partial y^+}$	$0 = \frac{1}{[\mathrm{PrRe}_\tau]} \frac{U^+}{U_b^+} + \frac{\partial^2 \Theta^+}{\partial (\mathrm{Pr} y^+)^2} + \frac{\partial R_{v\theta}^+}{\partial (\mathrm{Pr} y^+)}$
Meso layer	$0 = 1 + \frac{\partial^2 U^+}{\partial y^{\Lambda 2}} + \frac{\partial R_{vu}^\Lambda}{\partial y^\Lambda}$	$0 = \frac{U^+}{U_b^+} + \frac{\partial^2 \Theta^+}{\partial y^{\Lambda_\theta 2}} + \frac{\partial R_{v\theta}^{\Lambda_\theta}}{\partial y^{\Lambda_\theta}}$
Outer layer	$0 = 1 + \frac{1}{[\mathrm{Re}_\tau]} \frac{\partial^2 U^+}{\partial \eta^2} + \frac{\partial R_{vu}^+}{\partial \eta}$	$0 = \frac{U^+}{U_b^+} + \frac{1}{[\mathrm{PrRe}_\tau]} \frac{\partial^2 \Theta^+}{\partial \eta^2} + \frac{\partial R_{v\theta}^+}{\partial \eta}$

IV. SUMMARY AND CONCLUSIONS

A long-standing question in the study of the mean thermal energy balance (MHB) equation is the role of Prandtl number. One approach in clarifying the Prandtl number effect was developed in Refs. [15,16]. However, the role of Prandtl number has not yet been settled. An attempt at incorporating Prandtl number effect in scaling patch analysis is the introduction of scaled wall-normal distance as $y_\sigma = \eta(\mathrm{Pe}_\tau \theta_\tau)/(T_\mathrm{w} - T_\mathrm{c}) = (\mathrm{Pr} y^+)/\Theta_c^+$ [17]. A challenge in applying and interpreting y_σ is that it mixed the scaling of the wall-normal distance, y^+, and temperature, Θ_c^+. Another attempt to address the Prandtl number effect is the introduction of $yU_\infty/\nu\sqrt{\mathrm{St}}$ by Wang *et al.* [24], where U_∞ is the free streamwise velocity in turbulent boundary layer flows and St is the Stanton number. This scaling has also mixed the scaling of the wall-normal distance with the temperature through the Stanton number.

Another drawback in previous studies of turbulent heat transfer is the number of scaled variables and notation, which complicates the investigation of the problem. In the present work we minimize the number of rescaled variables and use simpler and more consistent notation. The multiscaling for different layers of turbulent channel heat transfer is summarized in Table II.

In the outer layer, mesolayer, and log law, the multiscaling of the MHB equation are analogous to those for the MMB equation. $\mathrm{Pe}_\tau = \mathrm{PrRe}_\tau$ in the MHB equation is the counterpart of Reynolds number Re_τ in the MMB equation. For the mean velocity and temperature deficit in the outer layer, we have shown that Zagarola-Smits-style scaling is a valid alternative to the traditional scaling. An interpretation of Zagarola-Smits-style scaling is provided. At infinite Reynolds number and Péclet number, Zagarola-Smits-style scaling is equivalent to the traditional scaling.

In the mesolayer, we have shown that scaling for the peak $R_{v\theta}$ location and value in the MHB equation exhibit close similarity to those for the R_{vu} in the MMB equation. The mesoscaled MHB equation is also analogous to the mesoscaled MMB equation. The effect of Prandtl number on the $R_{v\theta}$ peak location is the outward shifting due to the molecular thermal diffusion sublayer.

A form of the log law using $y^{+_\theta} = \mathrm{Pr} y^+$ is presented, consistent with the scaling of the MHB equation. The effect of Prandtl number on the log law is the shifting of the additive constant $B_\theta(\mathrm{Pr})$, which in turn is caused by the shifting of the molecular thermal diffusion sublayer and buffer layer with different Prandtl numbers.

Prandtl number is found to play a fundamental role in the scaling of MHB equation within the molecular thermal diffusion sublayer and buffer layer. At low Prandtl number $\mathrm{Pr} < 1$, a proper scaling of the wall-normal distance is $\mathrm{Pr}^{1/2} y^+$, the accompanying scaling for the mean temperature is $\Theta^+/\mathrm{Pr}^{1/2}$, and a relevant Péclet number is $\mathrm{Re}_\tau \mathrm{Pr}^{1/2}$. At very small Prandtl number $\mathrm{Pr} \ll 1$, the molecular thermal diffusion sublayer is much thicker than the viscous sublayer. At large Prandtl number $\mathrm{Pr} > 1$, a proper scaling of the wall-normal distance is $\mathrm{Pr}^{1/3} y^+$, the accompanying scaling

for the mean temperature is $\Theta^+/Pr^{2/3}$, and a relevant Péclet number is $Re_\tau Pr^{1/3}$. At ultra-high Prandtl number $Pr \gg 1$, the molecular thermal diffusion sublayer is buried deep inside the viscous sublayer.

ACKNOWLEDGMENT

The author is very grateful to Dr. Bernardini, Dr. Orlandi, Dr. Pirozzoli, and researchers from Dr. Kawamura's group, Dr. Abe, Dr. Matsuo, Dr. Kawamura, Dr. Kozuka, Dr. Seki, and Dr. Yamamoto, for generously sharing their DNS data.

[1] J. Kim and P. Moin, Transport of passive scalars in a turbulent channel flow, in *Turbulent Shear Flows 6*, (Springer-Verlag, Berlin, Heidelberg, 1989), pp. 85–96.
[2] H. Kawamura, K. Ohsaka, H. Abe, and K. Yamamoto, DNS of turbulent heat transfer in channel flow with low to medium-high Prandtl number fluid, Int. J. Heat Fluid Flow **19**, 482 (1998).
[3] Y. Na, D. V. Papavassiliou, and T. J. Hanratty, Use of direct numerical simulation to study the effect of Prandtl number on temperature fields, Int. J. Heat Fluid Flow **20**, 187 (1999).
[4] S. L. Lyons, T. J. Hanratty, and J. B. McLaughlin, Direct numerical simulation of passive heat transfer in a turbulent channel flow, Int. J. Heat Mass Transf. **34**, 1149 (1991).
[5] N. Kasagi, Y. Tomita, and A. Kuroda, Direct numerical simulation of passive scalar field in a turbulent channel flow, J. Heat Transfer **114**, 598 (1992).
[6] H. Kawamura, H. Abe, and K. Shingai, DNS of turbulence and heat transport in a channel flow with different Reynolds and Prandtl numbers and boundary conditions, in *Turbulence Heat Mass Transfer 3* (Proceedings of the Third Int. Symp. on Turbulence Heat and Mass Transfer) (Aichi Shuppan, 2000), pp. 15–32.
[7] H. Abe, H. Kawamura, and Y. Matsuo, Direct numerical simulation of a fully developed turbulent channel flow with respect to the Reynolds number dependence, J. Fluids Eng. **123**, 382 (2001).
[8] H. Abe, H. Kawamura, and Y. Matsuo, Surface heat-flux fluctuations in a turbulent channel flow up to $Re_\tau = 1020$ with $Pr = 0.025$ and 0.71, Int. J. Heat Fluid Flow **25**, 404 (2004).
[9] Y. Seki, K. Iwamoto, and H. Kawamura, Prandtl number effect on turbulence quantities through high spatial resolution DNS of turbulent heat transfer in a channel flow, in *ICHMT Digital Library Online* (Begel House, 2006), pp. 301–304.
[10] L. Redjem-Saad, M. Ould-Rouiss, and G. Lauriat, Direct numerical simulation of turbulent heat transfer in pipe flows: Effect of Prandtl number, Int. J. Heat Fluid Flow **28**, 847 (2007).
[11] H. Abe and R. A. Antonia, Scaling of normalized mean energy and scalar dissipation rates in a turbulent channel flow, Phys. Fluids **23**, 055104 (2011).
[12] C. Srinivasan and D. V. Papavassiliou, Heat transfer scaling close to the wall for turbulent channel flows, Appl. Mech. Rev. **65**, 031002 (2013).
[13] S. Pirozzoli, M. Bernardini, and P. Orlandi, Passive scalars in turbulent channel flow at high Reynolds number, J. Fluid Mech. **788**, 614 (2016).
[14] P. Fife, J. Klewicki, P. McMurtry, and T. Wei, Multiscaling in the presence of indeterminacy: Wall-induced turbulence, Multiscale Modeling Simulation **4**, 936 (2005).
[15] P. C. Fife, Scaling approaches to steady wall-induced turbulence, http://www.math.utah.edu/~fife/revarticle.pdf (2006).
[16] T. Wei, P. Fife, J. Klewicki, and P. McMurtry, Properties of the mean momentum balance in turbulent boundary layer, pipe and channel flows, J. Fluid Mech. **522**, 303 (2005).
[17] T. Wei, P. Fife, J. Klewicki, and P. McMurtry, Scaling heat transfer in fully developed turbulent channel flow, Int. J. Heat Mass Transf. **48**, 5284 (2005).
[18] H. Schlichting and K. Gersten, *Boundary-Layer Theory* (Springer, 2016).
[19] H. Tennekes and J. L. Lumley, *A First Course in Turbulence* (MIT Press, Cambridge, MA, 1972).

[20] A. S. Monin and A. M. Yaglom, *Statistical Fluid Mechanics, vol. I: Mechanics of Turbulence* (MIT Press, Cambridge, MA, 1965).
[21] S. Saha, J. C. Klewicki, A. S. H. Ooi, H. M. Blackburn, and T. Wei, Scaling properties of the equation for passive scalar transport in wall-bounded turbulent flows, Int. J. Heat Mass Transf. **70**, 779 (2014).
[22] S. Saha, J. C. Klewicki, A. S. H. Ooi, and H. M. Blackburn, Comparison of thermal scaling properties between turbulent pipe and channel flows via DNS, Int. J. Thermal Sci. **89**, 43 (2015).
[23] A. Zhou, S. Pirozzoli, and J. Klewicki, Mean equation based scaling analysis of fully-developed turbulent channel flow with uniform heat generation, Int. J. Heat Mass Transf. **115**, 50 (2017).
[24] X. Wang, L. Castillo, and G. Araya, Temperature scalings and profiles in forced convection turbulent boundary layers, J. Heat Transfer **130**, 021701 (2008).
[25] W. K. George and L. Castillo, Zero-pressure-gradient turbulent boundary layer, Appl. Mech. Rev. **50**, 689 (1997).
[26] A. Seena and N. Afzal, Intermediate scaling of turbulent momentum and heat transfer in a transitional rough channel, J. Heat Transfer **130**, 031701 (2008).
[27] A. Seena, A. Bushra, and N. Afzal, Logarithmic expansions for Reynolds shear stress and Reynolds heat flux in a turbulent channel flow, J. Heat Transfer **130**, 094501 (2008).
[28] S. B. Pope, *Turbulent Flows* (Cambridge University Press, Cambridge, 2001).
[29] T. L. Bergman and F. P. Incropera, *Fundamentals of Heat and Mass Transfer* (John Wiley & Sons, 2011).
[30] H. B. Squire, The friction temperature: A useful parameter in heat-transfer analysis, in *Proc. of General Discussion on Heat Transfer* (Institute of Mechanical Engineers, London, 1951), pp. 185–186.
[31] M. V. Zagarola and A. J. Smits, Mean-flow scaling of turbulent pipe flow, J. Fluid Mech. **373**, 33 (1998).
[32] T. Wei and Y. Maciel, Derivation of Zagarola-Smits scaling in zero-pressure-gradient turbulent boundary layers, Phys. Rev. Fluids **3**, 012601 (2018).
[33] H. M. Nagib and K. A. Chauhan, Variations of von Kármán coefficient in canonical flows, Phys. Fluids **20**, 101518 (2008).
[34] L. D. Landau and E. M. Lifshitz, *Fluid Mechanics*, Vol. 61 (Pergamon, New York, 1959).
[35] A. Izakson, On the formula for the velocity distribution near walls, Tech. Phys. USSR IV **2**, 155 (1937).
[36] C. B. Millikan, A critical discussion of turbulent flow in channels and circular tubes, in *Proc. 5th Int. Congress on Applied Mechanics (Cambridge, MA, 1938)* (Wiley, 1939), pp. 386–392.
[37] B. A. Kader and A. M. Yaglom, Heat and mass transfer laws for fully turbulent wall flows, Int. J. Heat Mass Transf. **15**, 2329 (1972).
[38] B. A. Kader, Temperature and concentration profiles in fully turbulent boundary layers, Int. J. Heat Mass Transf. **24**, 1541 (1981).
[39] V. G. Levich, *Physicochemical Hydrodynamics* (Prentice-Hall, New York, 1962).
[40] R. A. Gowen and J. W. Smith, The effect of the Prandtl number on temperature profiles for heat transfer in turbulent pipe flow, Chem. Eng. Sci. **22**, 1701 (1967).
[41] J. C. Neumann, Transfert de chaleur en régime turbulent pour les grands nombres de Prandtl, Information Aeraulique et Thermique **5**, 4 (1968).
[42] A. Fortier, Théorie asymptotique de la couche limite turbulente, in *Vortrag auf dem Kongreß für Strömungs-mechanik und Wärmeübertragung Sept* (Herceg-Novi, Yougoslovie, 1968).
[43] W. M. Kays and M. E. Crawford, *Convective Heat and Mass Transfer* (McGraw-Hill, New York, 1993).
[44] D. A. Shaw and T. J. Hanratty, Turbulent mass transfer rates to a wall for large Schmidt numbers, AIChE J. **23**, 28 (1977).
[45] Y.-H. Dong, X.-Y. Lu, and L.-X. Zhuang, Large eddy simulation of turbulent channel flow with mass transfer at high-Schmidt numbers, Int. J. Heat Mass Transf. **46**, 1529 (2003).
[46] M. Ould-Rouiss, M. Bousbai, and A. Mazouz, Large eddy simulation of turbulent heat transfer in pipe flows with respect to Reynolds and Prandtl number effects, Acta Mech. **224**, 1133 (2013).
[47] C. W. Kang and K.-S. Yang, Effects of Schmidt number on near-wall turbulent mass transfer in pipe flow, J. Mech. Sci. Technol. **28**, 5027 (2014).

[48] R. R. Long and T.-C. Chen, Experimental evidence for the existence of the 'mesolayer' in turbulent systems, J. Fluid Mech. **105**, 19 (1981).
[49] N. Afzal, Fully developed turbulent flow in a pipe: An intermediate layer, Arch. Appl. Mech. **52**, 355 (1982).
[50] N. Afzal, Mesolayer theory for turbulent flows, AIAA J. **22**, 437 (1984).
[51] K. R. Sreenivasan and A. Sahay, The persistence of viscous effects in the overlap region, and the mean velocity in turbulent pipe and channel flows, in *Self-Sustaining Mechanisms of Wall Turbulence*, edited by R. L. Panton, Advances in Fluid Mechanics (Computational Mechanics Publications, Southampton, UK, 1997), Vol. 15, pp. 253–272.
[52] M. Wosnik, L. Castillo, and W. K. George, A theory for turbulent pipe and channel flows, J. Fluid Mech. **421**, 115 (2000).
[53] K. R. Sreenivasan, The turbulent boundary layer, in *Frontiers in Experimental Fluid Mechanics*, edited by M. Gad-el-Hak (Springer, 1989), pp. 159–209.
[54] H. Kawamura, H. Abe, and Y. Matsuo, DNS of turbulent heat transfer in channel flow with respect to Reynolds and Prandtl number effects, Int. J. Heat Fluid Flow **20**, 196 (1999).
[55] P. Fife, T. Wei, J. Klewicki, and P. McMurtry, Stress gradient balance layers and scale hierarchies in wall-bounded turbulent flows, J. Fluid Mech. **532**, 165 (2005).
[56] T. Wei, P. McMurtry, J. Klewicki, and P. Fife, Mesoscaling of Reynolds shear stress in turbulent channel and pipe flows, AIAA J. **43**, 2350 (2005).